Tellus (2002), 54B, 395–406
Printed in UK. All rights reserved

TELLUS
ISSN 0280–6509

On the secondary meridional circulation associated with the quasi-biennial oscillation

By WOOKAP CHOI[1]*, HYUNAH LEE[1,2], WILLIAM B. GRANT[3], JAE H. PARK[3], JAMES R. HOLTON[4], KWANG-MOG LEE[5] and BARBARA NAUJOKAT[6], [1]*School of Earth and Environmental Sciences, College of Natural Sciences, Seoul National University, Seoul 151-742, Korea;* [2]*Atmospheric Chemistry Division, NCAR, 1850 Table Mesa Drive, Boulder, CO 80305, USA;* [3]*NASA Langley Research Center, MS 401A, Hampton, VA 23681-2199, USA;* [4]*Department of Atmospheric Sciences, University of Washington, Box 351640, Seattle, WA 98195, USA;* [5]*Department of Astronomy and Atmospheric Sciences, Kyungpook National University, Sankyuk-dong, Book-gu, Taegu, Korea;* [6]*Stratospheric Research Group, Institute for Meteorology, Free University Berlin, D-12165 Berlin, Germany*

(Manuscript received 29 January 2001; in final form 14 May 2002)

ABSTRACT

Concentrations and distributions of stratospheric aerosol, hydrogen fluoride and ozone from the Halogen Occultation Experiment (HALOE) on the Upper Atmosphere Research Satellite (UARS) are used to investigate features associated with transport by the secondary meridional circulation induced by the quasi-biennial oscillation (QBO). The points of maxima in the divergence and convergence of the QBO-induced meridional velocity at the equator are identified from the meridional gradients of the tracers. Such points can be identified from the tracer fields in the westerly shear zones but not in the easterly shear zones. The temporal variation of tracer concentration at the equator is determined mainly by vertical advection, which is significantly larger during the westerly shear phase of the QBO than during the easterly shear phase, since the QBO-induced equatorial sinking motion amplifies the vertical gradient. Thus, the vertical advection associated with the secondary circulation has a stronger influence on the equatorial tracer variation during the westerly shear phase than during the easterly shear phase.

1. Introduction

The meridional circulation in the stratosphere that determines the distributions of long-lived chemical species is the so-called Brewer–Dobson circulation or residual circulation (e.g., Holton, 1986). The residual circulation, which is characterized by rising in the low-latitude region, poleward drift and sinking in the high-latitude region, has been calculated by using the thermodynamic energy equation (e.g., Rosenlof, 1995; Eluszkiewicz et al., 1996; Randel et al., 1999) or the zonal momentum equation (e.g., Rosenlof and Holton, 1993). The residual circulation estimated by either method was obtained for nominal atmospheric conditions and thus should represent the sum of the planetary-scale extratropically driven mean equator-to-pole circulation and the secondary circulations associated with the equatorial semiannual oscillation (SAO) and the QBO. Unfortunately, residual circulations calculated by the previously mentioned authors do not show evidence of the QBO secondary circulation probably because of the poor vertical resolution of the data. However, the existence of this secondary circulation can be detected in the tracer distributions in the equatorial region. The secondary circulation associated with the equatorial QBO and its influence on the distributions of dynamic variables and tracers have been extensively studied. The typical tracers studied for influence of the secondary circulation are ozone, aerosol, CH_4, H_2O, N_2O, and NO_2. For ozone, the works are found, for example, in

*Corresponding author.
e-mail: wchoi@snu.ac.kr

Bowman (1989), Zawodny and McCormick (1991), Chipperfield and Gray (1992), Gray and Ruth (1993), Hasebe (1994), Randel and Wu (1996), Jones et al. (1998), Nagashima et al. (1998), and Kinnersley and Tung (1999); for aerosol, in Trepte and Hitchman (1992), Hasebe (1994), Hitchman et al. (1994), and Choi et al. (1998); for CH_4, in Ruth et al. (1997), Randel et al. (1998), and Gray and Russell (1999); for H_2O, in O'Sullivan and Dunkerton (1997), Randel et al. (1998), and Gray and Russell (1999); for N_2O, in Chipperfield and Gray (1992), Kennaugh et al. (1997), O'Sullivan and Dunkerton (1997), and Jones et al. (1998); for NO_2, in Zawodny and McCormick (1991), and Chipperfield and Gray (1992). The potential vorticity (Hitchman and Leovy, 1986) and momentum (Takahashi and Boville, 1992; Baldwin and Tung, 1994; Takahashi, 1996) have also been studied in association with the QBO circulation. Recently, Niwano and Shiotani (2001) estimated the vertical velocity at the equator associated with the QBO from total water ($[H_2O] + 2[CH_4]$), and it shows larger QBO variations than the residual circulation does. All of the aspects of the QBO, including the secondary circulation, are reviewed by Baldwin et al. (2001).

A double-peak structure of tracer distributions, with an equatorial minimum or maximum value of tracers, is evidence of the existence of the secondary circulation. The double-peak structure observed in both the upper and lower stratosphere is one of the distinctive features of the tracer distribution observed in the meridional plane of the tropical stratosphere. The double-peak structure in the upper stratosphere is produced by the equatorial sinking motion associated with the SAO in the zonal wind (Jones and Pyle, 1984; Holton and Choi, 1988; Ruth et al., 1997). A double-peak structure is also observed in the lower stratosphere and is associated with the QBO of the equatorial zonal wind. It has been observed in the distributions of long-lived chemical species such as N_2O, H_2O, NO_2 and aerosol (Trepte and Hitchman, 1992; Hasebe, 1994; O'Sullivan and Dunkerton, 1997; Choi et al., 1998). The double-peak structure is usually identified in the latitude-altitude cross-sections, but it can also be identified in the time–latitude sections at various altitudes such as those shown in Plate 2 of Choi et al. (1998).

The double peak comprises lower values at the equator and higher values near the edges of the tropics for such tracers as aerosol and CH_4, which have tropospheric sources, while the reverse pattern is found for such tracers as HF and HCl, which have upper-stratospheric sources. The double-peak structure is produced by differences in vertical velocities between the equator and the edges of the subtropics. Formation of the double peaks is caused by sinking at the equator, relative to the subtropics, which is necessary for maintaining the warm thermal anomaly at the equator associated with the QBO westerly shear. This equatorial sinking and the resulting meridional motion constitute a secondary circulation of the QBO (Reed, 1964; Dickinson, 1968; Plumb and Bell, 1982; Gray and Pyle, 1989; Trepte and Hitchman, 1992). Although the secondary meridional circulation is a well-known feature in two-dimensional model simulations (e.g., Plumb and Bell, 1982; Politowicz and Hitchman, 1997; Jones et al., 1998), it is difficult to observe directly. However, the influences of the QBO secondary circulation on tracer distributions are easily observed as double-peak structures.

In this study we use distributions of tracers such as aerosol, HF, and ozone to investigate the characteristic features of the secondary circulation associated with the QBO. We have two objectives in this study. The first objective is to identify double-peak structures from multi-year observations of long-lived chemical species and to associate those structures with the secondary meridional circulation. The double-peak structures appear only during the westerly shear period. The influences of the secondary circulation on tracer distributions during the easterly shear period are more subtle. The second objective in this study is to find the reason for the differences in the influences of the secondary circulation between the westerly and easterly shear phases.

In Section 2 we show how to identify the double-peak structures from the observation of aerosols and hydrogen fluoride (HF). In Section 3 we define the maximum convergence and divergence points at the equator associated with the secondary circulation. We also discuss the asymmetry observed in the tracer fields between westerly and easterly shear phases. In Section 4 we discuss the differences in the vertical gradient of tracer distributions during the westerly and easterly shear phases and their influences on tracer distributions.

2. Signs of the secondary circulation observed in tracer distributions

The schematic diagram of the secondary meridional circulation associated with the zonal wind is shown in

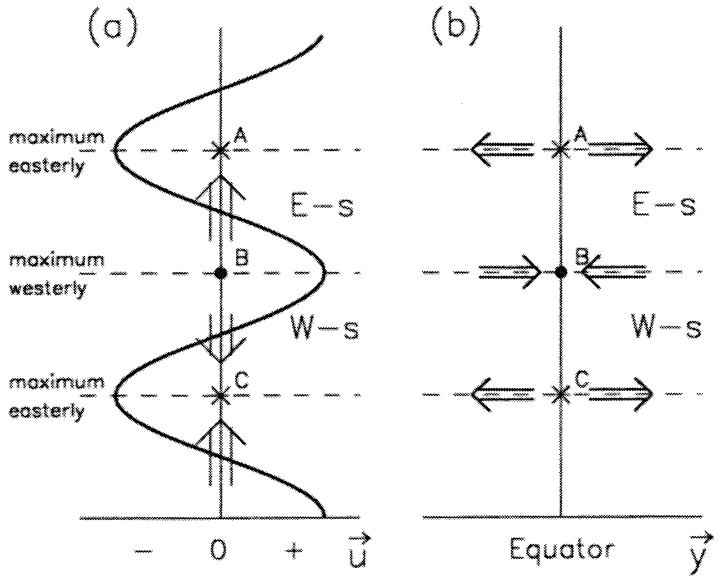

Fig. 1. Schematic vertical profiles of (a) the zonal wind and vertical velocity and (b) the meridional divergence. Divergence and convergence points are denoted by asterisks and dots, respectively. W-s and E-s represent westerly and easterly shear zones, respectively.

Fig. 1, which is adapted from the model of Plumb and Bell (1982). For simple interpretation, the zonal wind is assumed to be sinusoidal in the vertical direction. The thermal wind relationship requires a warm anomaly in the westerly shear zone and a cold anomaly in the easterly shear zone. To maintain these temperature anomalies there exist regions of relative sinking and rising motions in the westerly and easterly shear zones. In this ideal distribution of zonal wind, the maximum sinking (rising) motion appears in the maximum westerly (easterly) shear zone, which coincides with the zero zonal wind level. The location of the maximum easterly (westerly) wind coincides with that of the maximum horizontal divergence (convergence). Hereafter, we call the point of maximum horizontal divergence denoted by either A or C in Fig. 1 as a divergence point and the point of maximum horizontal convergence denoted by B as a convergence point.

The total residual circulation is the sum of the QBO-induced vertical circulation shown in Fig. 1 and the background annually varying, extratropically driven residual circulation. A double-peak structure in tracers is expected at levels near the points A or C, where owing to the QBO circulation, the vertical velocity of the total residual circulation is weaker at the equator than in the subtropics. We estimate the location of such points from the observed distribution of tracers in data from the HALOE. Since the HALOE observations use the solar occultation technique and thus cannot produce synoptic maps of global tracer concentrations, the observed values were interpolated to the 15th of each month. We assume here that these are representative of monthly mean values.

2.1. Aerosols

First we use distributions of aerosol extinction coefficients. These are especially suitable for our purposes since they had large vertical gradients after the eruption of Mount Pinatubo (Choi et al., 1998). The double-peak structures are very obvious in the aerosol data, and the convergence and divergence points are easily located. By contrast, for tracers with small vertical gradients, the shape of contour lines could have large errors due to the uncertainty of the satellite observations.

The latitude-altitude cross-section of aerosol extinction coefficients was plotted in each month to locate divergence and convergence points. We used only the component of the field symmetric about the equator, which made identification of those points easier. Although the QBO-induced circulation is stronger in the winter hemisphere (Jones et al., 1998; Kinnersley

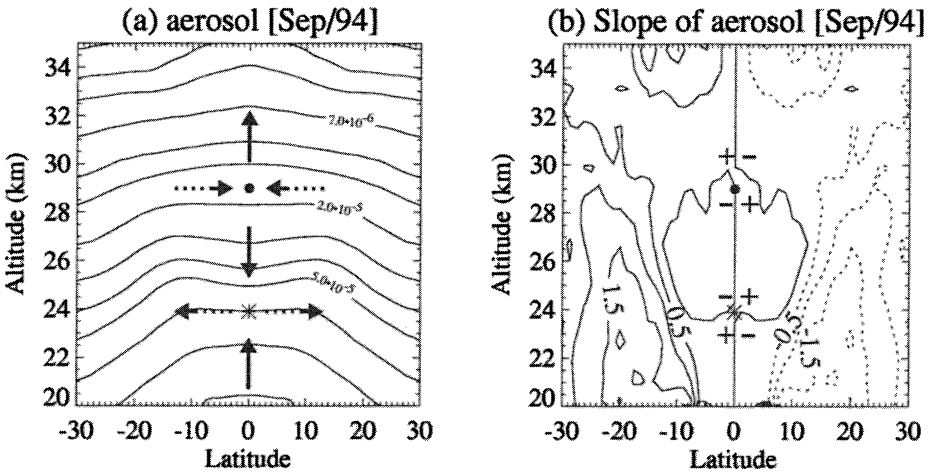

Fig. 2. Symmetric fields of (a) aerosol extinction coefficient (km^{-1}) and (b) its slope (m km^{-1}) in the meridional plane for September 1994. Solid and dotted arrows denote the secondary vertical and horizontal motions. Plus and minus signs represent the slopes near the convergence and divergence points.

and Tung, 1999; Randel et al., 1999), it is mainly for the subtropics and extratropics. The features near the equator are close to symmetric (Wallace, 1973; Dunkerton and Delisi, 1985; see also Plate 2 of Choi et al., 1998). In Figs. 2a and 2b an example of the symmetric field of aerosol extinction coefficients and the slopes of the contour lines of the constant extinction coefficient in the meridional plane are shown, respectively. In the slope patterns, the divergence and convergence points are shown as the points of slope reversal. The divergence point denoted by an asterisk is located between the negative-to-positive gradient reversal in the Northern Hemisphere and the positive-to-negative gradient reversal in the Southern Hemisphere. The convergence point denoted by a dot, on the other hand, is located between the positive-to-negative gradient reversal in the Northern Hemisphere and the negative-to-positive gradient reversal in the Southern Hemisphere. During September 1994, the month shown in Fig. 2, a westerly shear zone is present in the lower stratosphere (see Fig. 5 for the zonal wind). The locations of the dot and the asterisk in Fig. 2, therefore, correspond to B and C in Fig. 1, respectively. The solid and dotted arrows in Fig. 2a represent the secondary vertical and horizontal motions associated with the QBO.

2.2. HF

Although the field of the aerosol extinction coefficient seems to show the effects of the QBO meridional circulation pattern very well, aerosol extinction is not a conserved property like the mixing ratio of a molecular species. To see whether a similar pattern exists in the distribution of a molecular species, we analyzed the distributions of the HF mixing ratio observed by the HALOE. HF is produced in the upper stratosphere and is a quasi-conservative tracer in the lower stratosphere (Russell et al., 1996). The symmetric distribution of the HF mixing ratio and the slope of the contour lines in the meridional plane are shown during the westerly shear phase in September 1994 in Fig. 3. The locations of the convergence and divergence points are identified by distribution of the slopes and are similar to the locations of the two points in Fig. 2, although the vertical distance between the two points in Fig. 3 is slightly shorter. As seen in Figs. 2 and 3, we can identify the points of meridional divergence by examining the slope of contour lines during the westerly shear phase.

To see whether the same technique can be used to estimate the QBO-induced meridional circulation during the easterly shear phase of the QBO, the HF distribution and its slope are shown in Fig. 4 during the month of the easterly shear in September 1993. As Fig. 1 shows, there should be a pair of divergence and convergence points (A and B) related to the easterly shear zone. However, the secondary vertical rising superposed on the background rising motion makes the distribution in Fig. 4a appear to be similar to the distribution produced by the background rising alone. The

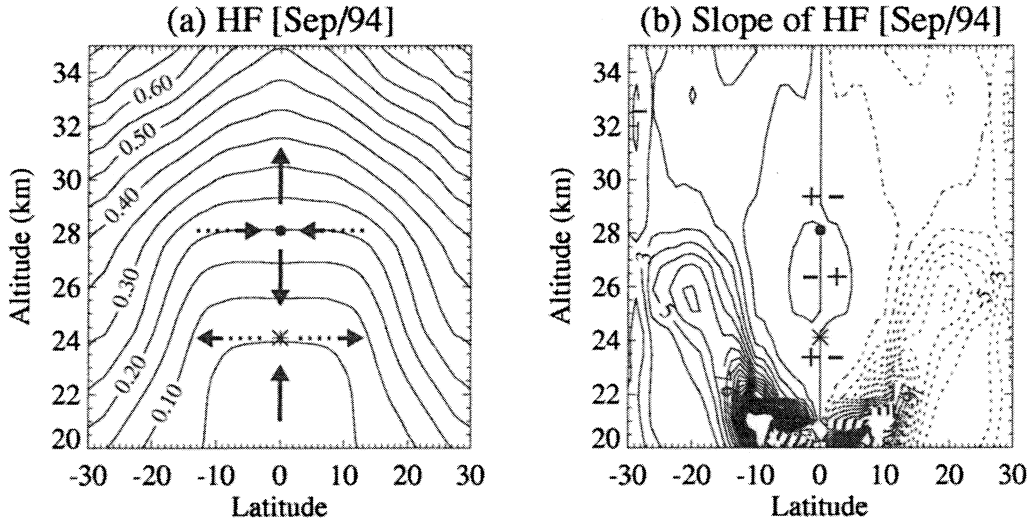

Fig. 3. Same as in Fig. 2 but for HF mixing ratio (ppbv).

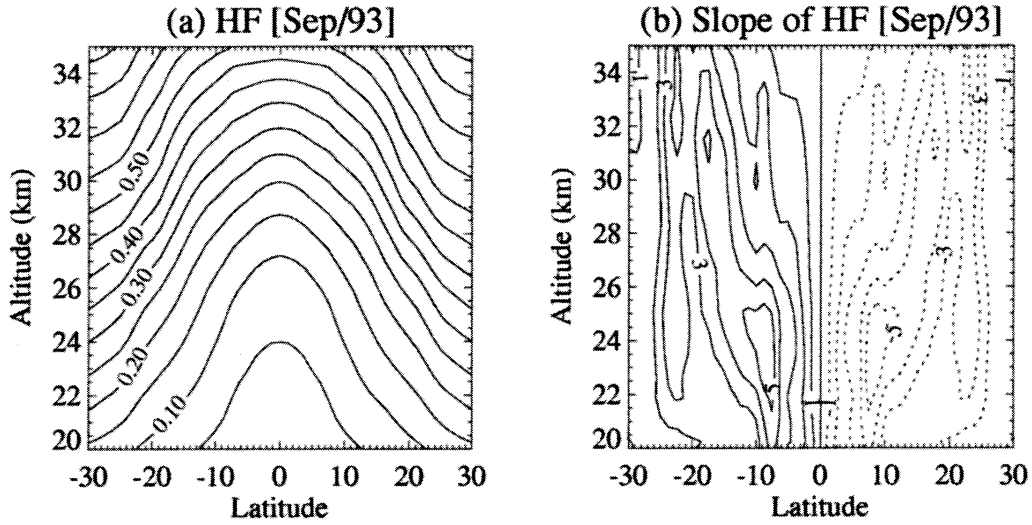

Fig. 4. Same as in Fig. 3 but for September 1993.

slope in Fig. 4b does not show a reversal of gradient as in Figs. 2b and 3b; therefore, it is difficult to identify signs of the QBO secondary circulation in the easterly shear zone. The lack of an equatorial sinking motion in the secondary circulation in the easterly shear phase means that no double-peak pattern appears. Furthermore, the vertical gradient of the mixing ratio at the equator during the easterly shear phase is smaller than that during the westerly shear phase; thus, the contribution to the mixing ratio distribution from the QBO circulation is smaller. It seems that variations associated with enhanced rising motion are hard to observe by satellite remote sensing when the spatial gradient of tracer concentration is relatively small. The reason for the relatively weak signal of the QBO secondary circulation that is observed in tracer distributions during the easterly shear period is discussed in a later section.

3. Points of meridional divergence and convergence in westerly and easterly shear zones

The divergence and convergence points were identified for aerosol and HF each month by using the slope in the meridional plane, as discussed in Section 2. Those points are shown in Fig. 5. To see if those observed points are associated with the secondary circulation, the estimated vertical velocity and the meridional divergence associated with the QBO in Singapore zonal winds are shown in Figs. 5a and 5b, respectively (from Choi et al., 1998).

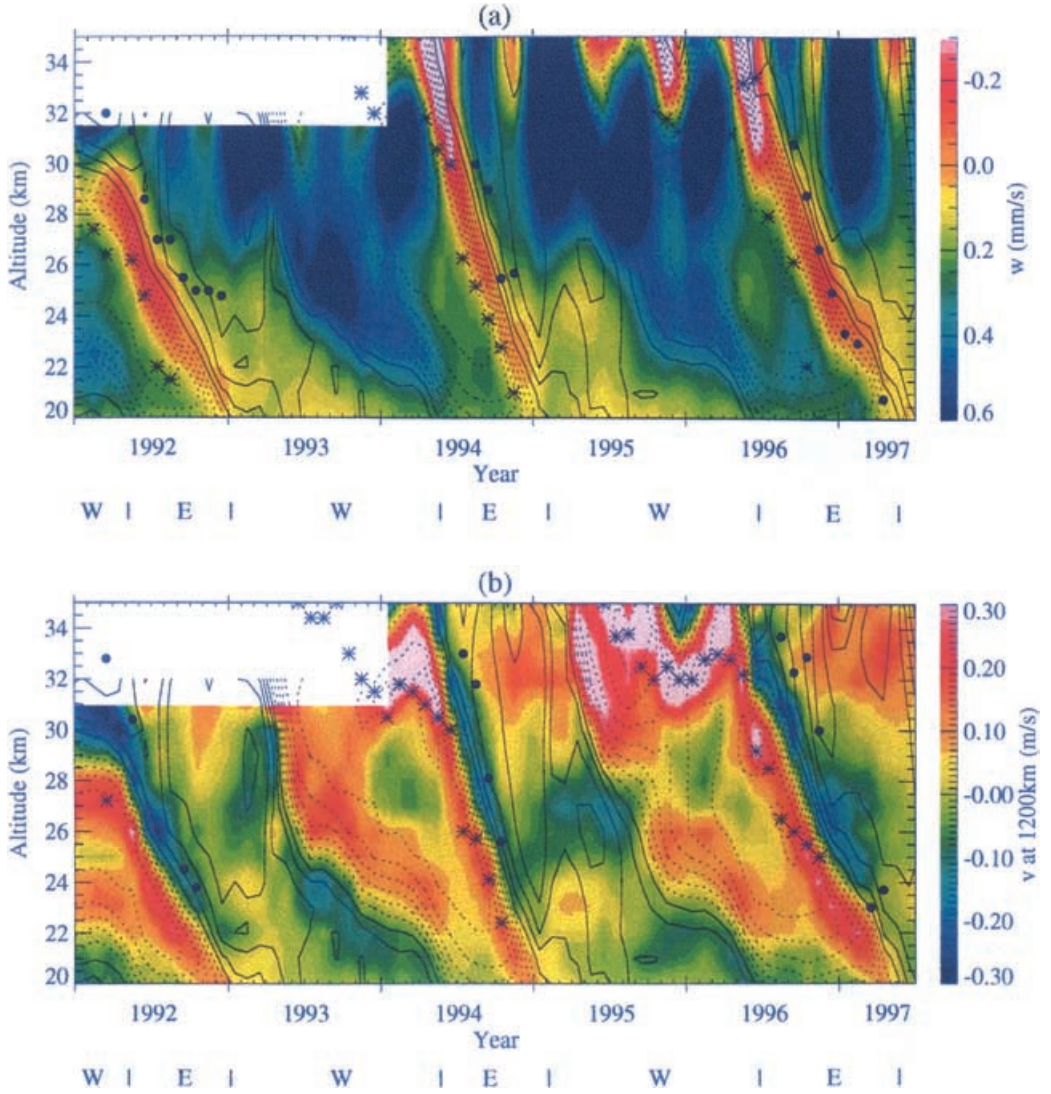

Fig. 5. (a) Estimated equatorial vertical velocity is shown in color. Divergence and convergence points observed from the aerosol distribution are also shown as asterisks and dots, respectively. (b) Estimated equatorial meridional divergence multiplied by 1200 km is shown in color. Divergence and convergence points observed from HF are shown as asterisks and dots. Contour lines denote zonal wind (m s^{-1}) in both panels. W and E represent westerly and easterly periods at the lowest level, respectively.

In Choi et al. (1998) the residual mean vertical velocity at the equator, w, was obtained by using an approximate form of the thermodynamic energy equation in the log-pressure coordinate system

$$w\left(\frac{\kappa T}{H}+\frac{\partial T}{\partial z}\right)\approx q-\alpha\delta T_{\mathrm{B}} \tag{1}$$

where κ is R/c_p, R is the gas constant, c_p is the specific heat at constant pressure, T is the temperature, H is the scale height, q is the monthly mean heating rate, and α is the Newtonian cooling rate. All the variables are zonal mean values, and overbars are omitted for simplicity. δT_{B} is the equatorial temperature anomaly associated with the QBO, and by using the thermal wind relationship it can be written approximately as (Andrews et al., 1987; Baldwin et al., 2001)

$$\delta T_{\mathrm{B}}\approx\frac{L^2H\beta}{R}\frac{\partial u}{\partial z} \tag{2}$$

where L is the meridional scale of the QBO, β is $2\Omega/a$, Ω is the angular velocity, a is the radius of the Earth, and u is the zonal wind velocity. Randel et al. (1999) suggested that this technique provides an easy method to estimate the anomaly of the equatorial vertical velocity. The magnitudes of the maxima and minima of the vertical velocity shown in Fig. 5a are slightly larger than those estimated by Niwano and Shiotani (2001). The QBO amplitudes of the vertical velocity are about 0.2 and 0.3 mm s^{-1} at 40 and 30 hPa, respectively, while Niwano and Shiotani (2001) showed the amplitude of about 0.15 and 0.2 mm s^{-1} on those levels. The QBO amplitude used here might have been overestimated due to uncertainties of the meridional scale and the Newtonian cooling coefficients as well as the monthly mean heating rates. Choi et al. (1998) used 1200 km for the meridional scale following Andrews et al. (1987) and 50 days at 20 km and 10 days at 35 km for the Newtonian cooling time scale. Randel et al. (1999) suggested 1000–1200 km for the meridional length scale and 50 and 6 days on the lower and upper stratosphere for the radiative cooling time scales.

The meridional divergence is obtained from the vertical velocity through the continuity equation

$$\frac{\partial v}{\partial y}=\frac{w}{H}-\frac{\partial w}{\partial z}. \tag{3}$$

Equation (3) can be approximated as $\partial v/\partial y\approx -\partial w/\partial z$, since w/H is negligible. By using Eqs. (1) and (3), the meridional divergence can be written as

$$\frac{\partial v}{\partial y}\approx-\frac{\partial}{\partial z}\left(\frac{q}{\kappa T/H+\partial T/\partial z}\right)+\frac{\partial}{\partial z}\left(\frac{\alpha\delta T_{\mathrm{B}}}{\kappa T/H+\partial T/\partial z}\right). \tag{4}$$

The first term in the right-hand side of Eq. (4) turns out to be very small below about 28 km. Thus, using Eqs. (2) and (4) the meridional divergence can be written as

$$\frac{\partial v}{\partial y}\approx\frac{\alpha L^2H\beta}{R}\frac{\partial}{\partial z}\left(\frac{\partial u/\partial z}{\kappa T/H+\partial T/\partial z}\right) \tag{5}$$

below the 28 km level. In deriving Eq. (5) the vertical change of the Newtonian cooling rates is neglected, since its contribution is small. The meridional divergence was calculated by using Eqs. (3) and (5), and they gave similar results below about 28 km.

The vertical velocity in Eq. (1) is dependent on the Newtonian cooling rates and the meridional scale L as well as monthly mean heating rates q. If the heating rates were inaccurate, then the vertical velocity could also be inaccurate and even have a wrong sign. There are many uncertainties in obtaining q in the equatorial lower stratosphere, and the resulting errors in q could give rise to under- or overestimation of the vertical velocity. The meridional divergence, however, is less dependent on the monthly mean heating rates as seen in Eq. (5). Although the magnitude of the meridional divergence is sensitive to the choice of Newtonian cooling rate and the meridional scale, the sign is determined only by observed wind and temperature. Thus, the sign of the estimated meridional divergence (divergence or convergence) should be more certain than the sign of the estimated vertical velocity (rising or sinking).

The meridional divergence was multiplied by 1200 km to approximate the poleward velocity at 1200 km from the equator. For reference in Fig. 5, the zonal wind observed in Singapore is also shown by contour lines. The divergence and convergence points in Fig. 5 are located in the westerly shear zones in 1992, 1994, and 1996 for both aerosol and HF. In the easterly shear phases, however, these points were difficult to identify for the reasons discussed previously. The locations of the pair of divergence and convergence points shown in Fig. 5a correspond to C and B in Fig. 1. They are in good agreement with the estimated

vertical velocity. Fig. 5b shows that the locations of the divergence and convergence points are also in good agreement with the estimated divergence at the westerly shear zones. Although the estimated divergence at the easterly shear zone is in comparable magnitude with that at the westerly shear zone, no equivalent points are identified during the easterly shear phases.

The locations of the divergence points coincide approximately with the easterly wind maxima, but the convergence points do not coincide with the westerly wind maxima. To explain why the location of convergence points does not coincide with the maximum westerly winds, the vertical profiles of zonal wind are shown for months of the westerly shear phase and the easterly shear phase in Figs. 6a and 6b, respectively. The shape of the vertical profile of the easterly wind is close to sinusoidal, and the theory in Fig. 1 is easily applied. The shape of the westerly wind, however, is not sinusoidal, and thus the convergence points are not located at the maximum westerly wind region. Politowicz and Hitchman (1997) gave a useful discussion for non-sinusoidal zonal wind profiles. In Fig. 6 the estimated divergence is also shown. The magnitudes of estimated divergence are comparable between westerly and easterly shear zones, although the pair of divergence and convergence points is identified only in the westerly shear phase.

4. Differences in the vertical advection due to the vertical gradient

The estimated divergence and convergence during the easterly shear phases shown in Fig. 5b are as strong as those during the westerly shear phase. However, the sign of the secondary circulation is difficult to observe. We believe this is caused by the smaller spatial gradient, especially the vertical gradient, during the easterly shear phases. The satellite remote sensing does not resolve small variation of tracer concentrations; therefore, the shapes of contour lines have a certain degree of uncertainty. The double-peak structure is more easily observed in aerosol (Fig. 2a) than in HF (Fig. 3a) because the vertical gradient of the aerosol extinction coefficient is larger than that of HF. To examine the temporal variation of the vertical gradient, we show ozone mixing ratio (contour lines) and its vertical gradient (in color) at the equator in Fig. 7. We show the ozone distribution instead of HF

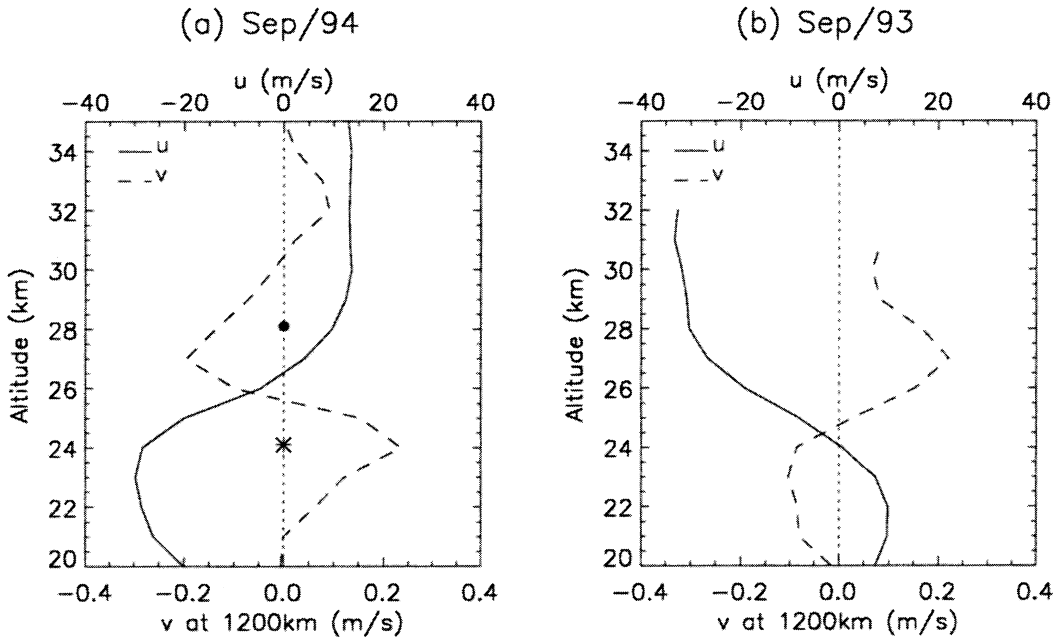

Fig. 6. Vertical profiles of zonal wind and estimated meridional velocity at 1200 km from the equator in (a) September 1994 and (b) September 1993 with a divergence point (asterisk) and a convergence point (dot).

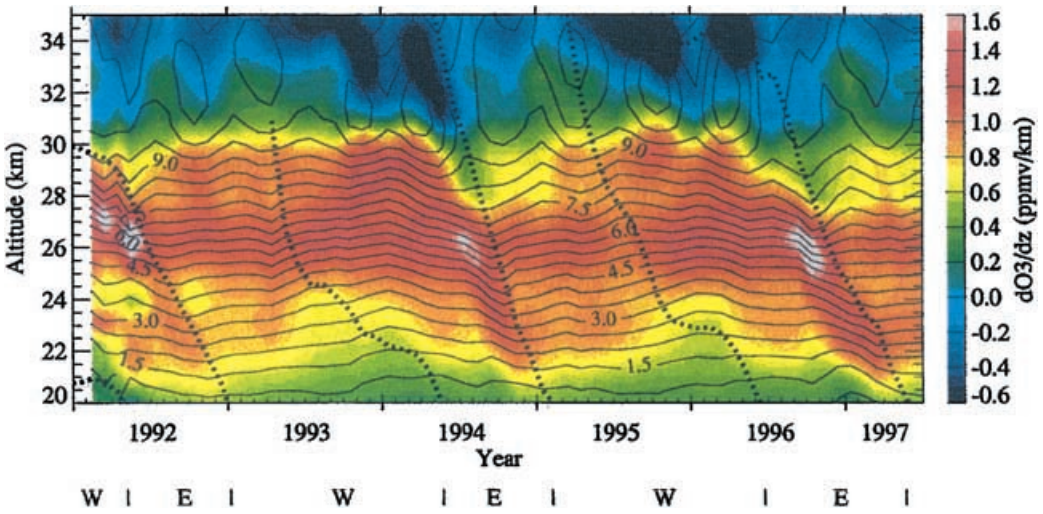

Fig. 7. Mixing ratio of ozone (solid contour, ppmv) and its vertical gradient (in color) at the equator. Dotted lines mark boundaries between regions of easterly (E) and westerly (W) QBO regimes.

because it has the largest vertical gradient of mixing ratio among trace gas species. The vertical gradient of O_3 is large in the lower stratosphere so that its change, due to the QBO, is more pronounced than that in HF mixing ratio (see also Cordero et al., 1997). The contour lines of the ozone mixing ratio show downward propagation of higher values in time following the westerly shear zones in 1994 and 1996–1997. The change of the vertical gradient at the equator along the westerly shear is clearly seen in the figure. The vertical gradient is distinctively larger during the westerly shear phase. The larger gradient yields the larger change in mixing ratio by the effect of the vertical advection.

To explain the relationship between the vertical gradient of ozone and the secondary vertical velocity associated with the QBO, a schematic diagram is shown in Fig. 8. In the westerly shear zone in Fig. 8a, the sinking motion above the divergence point (or maximum easterly) makes the vertical gradient larger. The relative downward motion, combined with the already amplified gradient, produces a large increase in concentration. In the easterly shear zone in Fig. 8b, however, the enhanced upward motion above the convergence point does not increase the vertical gradient, but sometimes decreases it. Thus, the extra upward motion owing to the QBO does not change the concentration much because the vertical gradient is comparatively small. By this reasoning, the pairs of divergence and convergence points are easy to observe during the westerly shear phase and difficult to observe during the easterly shear phase, even though the strengths of the estimated divergence and convergence are similar.

5. Summary and discussion

The effects of secondary vertical motion at the equator and the associated meridional divergence associated with the QBO in tracer distributions were examined by using HALOE observations of aerosols, HF, and ozone. The secondary circulation makes a pair of convergence and divergence points at the equator, and these propagate downward in time with the shear zones. These pairs are easily located from concentrations of aerosol and HF in the westerly shear zones but not in the easterly shear zones. The location of the divergence point is in good agreement with that of the maximum easterly winds, while the convergence point does not coincide exactly with the maximum westerly winds. The reason for this difference is that the vertical profile of the easterly wind is close to sinusoidal, while the westerly is not.

The double-peak structures observed in the distributions of long-lived chemical species in the

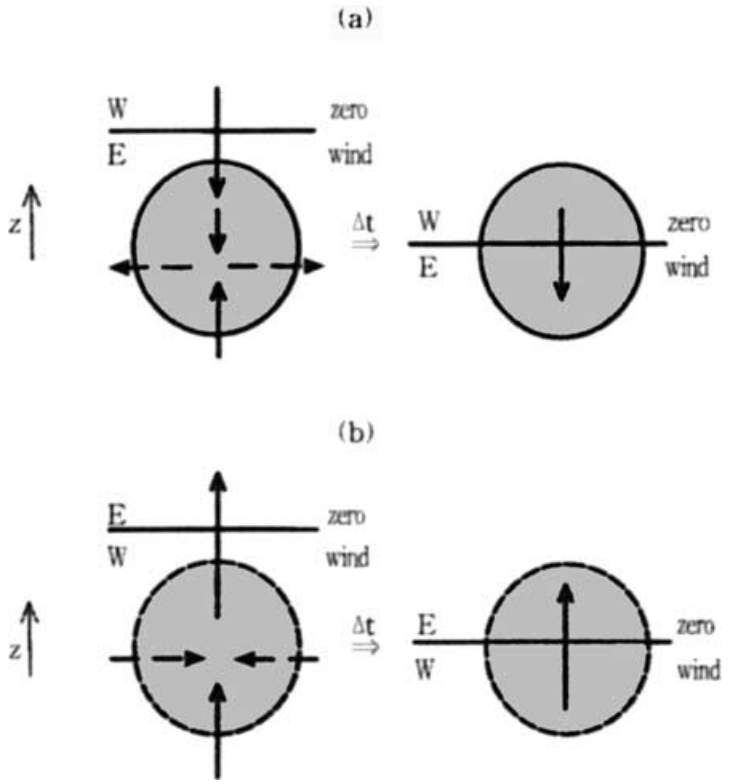

Fig. 8. Schematic diagram for interpretation of the convergence and divergence pattern for (a) westerly and (b) easterly shear phases. The solid line is the level of zero wind and the shaded area is the region of interest. Solid and dashed arrows represent the QBO-induced vertical and meridional velocities, respectively. The length of the arrows represents relative speed of the circulation.

lower stratosphere have long been recognized to be associated with the secondary circulation of the QBO. Those structures appear only during the westerly shear phases and are a result of the upper level convergence and the lower level divergence. The convergence and divergence points are produced by the secondary circulation, and the vertical gradient changes accordingly. During the westerly shear phase, downward motion enhances the vertical gradient of the mixing ratio and thus magnifies the effect of vertical advection. In the easterly shear zone, the rising motion makes the vertical gradient smaller, and thus the resulting change of concentration is small. Since the tracers have small vertical gradients during the easterly shear phase, a secondary circulation of comparable magnitude to that during the westerly phase would produce a much smaller signature in the tracer distributions. Thus, the vertical advection associated with the secondary circulation has a stronger influence on the equatorial tracer variation during the westerly shear phase than during the easterly shear phase.

6. Acknowledgements

We are grateful to the HALOE project team for providing the HALOE data and to W. J. Randel for helpful discussions. We are also grateful to an anonymous reviewer for many helpful suggestions, which made the manuscript clearer. The work in the US was supported by NASA and in Korea by the Ministry of Science and Technology and the Climate Environment System Research Center sponsored by the SRC program of the Korean Science and Engineering Foundation. W. C. was supported by the BK21 program of the Ministry of Education of Korea. J. R. H. was supported by NASA grant NAG5-7090 (UARS).

Support for W. C. and K.M.x L. for time spent at the NASA Langley Research Center to do the work reported in this paper was provided by NASA Grant NAS1-19656.

REFERENCES

Andrews, D. G., Holton, J. R. and Leovy, C. B. 1987. *Middle atmosphere dynamics*. Academic Press, 489 pp.

Baldwin, M. P. and Tung, K. K. 1994. Extra-tropical QBO signals in angular momentum and wave forcing. *Geophys. Res. Lett.* **21**, 2717–2720.

Baldwin, M. P., Gray, L. J., Dunkerton, T. J., Hamilton, K., Haynes, P. H., Randel, W. J., Holton, J. R., Alexander, M. J., Hirota, I., Horinouchi, T., Jones, D. B. A., Kinnersley, J. S., Marquardt, C., Sato, K. and Takahashi, M. 2001. The quasi-biennial oscillation. *Rev. Geophys.* **39**, 179–229.

Bowman, K. P. 1989. Global patterns of the quasi-biennial oscillation in total ozone. *J. Atmos. Sci.* **46**, 3328–3343.

Chipperfield, M. P. and Gray, L. J. 1992. Two-dimensional model studies of the interannual variability of trace gases in the middle atmosphere. *J. Geophys. Res.* **97**, 5963–5980.

Choi, W., Grant, W. B., Park, J. H., Lee, K.-M., Lee, H. and Russell, J. M., III. 1998. Role of the quasi-biennial oscillation in the transport of aerosols from the tropical stratospheric reservoir to midlatitudes. *J. Geophys. Res.* **103**, 6033–6042.

Cordero, E. C., Kawa, S. R. and Schoeberl, M. R. 1997. An analysis of tropical transport: Influence of the quasi-biennial oscillation. *J. Geophys. Res.* **102**, 16,453–16,461.

Dickinson, R. E. 1968. On the excitation and propagation of zonal winds in an atmosphere with Newtonian cooling. *J. Atmos. Sci.* **25**, 269–279.

Dunkerton, T. J. and Delisi, D. P. 1985. Climatology of the equatorial lower stratosphere. *J. Atmos. Sci.* **42**, 376–396.

Eluszkiewicz, J., Crisp, D., Zurek, R., Elson, L., Fishbein, E., Froidevaux, L., Waters, J., Grainger, R. G., Lambert, A., Harwood, R. and Peckham, G. 1996. Residual circulation in the stratosphere and lower mesosphere as diagnosed from Microwave Limb Sounder data. *J. Atmos. Sci.* **53**, 217–240.

Gray, L. J. and Pyle, J. A. 1989. A two-dimensional model of the quasi-biennial oscillation of ozone. *J. Atmos. Sci.* **46**, 203–220.

Gray, L. J. and Russell, J. M., III. 1999. Interannual variability of trace gases in the subtropical winter stratosphere. *J. Atmos. Sci.* **56**, 977–993.

Gray, L. J. and Ruth, S. 1993. The modeled latitudinal distribution of the ozone quasi-biennial oscillation using observed equatorial winds. *J. Atmos. Sci.* **50**, 1033–1046.

Hasebe, F. 1994. Quasi-biennial oscillations of ozone and diabatic circulation in the equatorial stratosphere. *J. Atmos. Sci.* **51**, 729–745.

Hitchman, M. H. and Leovy, C. B. 1986. Evolution of the zonal mean state in the equatorial middle atmosphere during October 1978–May 1979. *J. Atmos. Sci.* **43**, 3159–3176.

Hitchman, M. H., McKay, M. and Trepte, C. R. 1994. A climatology of stratospheric aerosol. *J. Geophys. Res.* **99**, 20,689–20,700.

Holton, J. R. 1986. Meridional distribution of stratospheric trace constituents. *J. Atmos. Sci.* **43**, 1238–1242.

Holton, J. R. and Choi, W. 1988. Transport circulation deduced from SAMS species data. *J. Atmos. Sci.* **45**, 1929–1939.

Jones, R. L. and Pyle, J. A. 1984. Observations of CH_4 and N_2O by the Nimbus 7 SAMS: A comparison with in situ data and two-dimensional numerical model calculations. *J. Geophys. Res.* **89**, 5263–5279.

Jones, D. B. A., Schneider, H. R. and McElroy, M. B. 1998. Effects of the quasi-biennial oscillation on the zonally averaged transport of tracers. *J. Geophys. Res.* **103**, 11,235–11,249.

Kennaugh, R., Ruth, S. and Gray, L. J. 1997. Modeling quasi-biennial variability in the semiannual double peak. *J. Geophys. Res.* **102**, 16,169–16,187.

Kinnersley, J. S. and Tung, K. K. 1999. Mechanisms for the extratropical QBO in circulation and ozone. *J. Atmos. Sci.* **56**, 1942–1962.

Nagashima, T., Takahashi, M. and Hasebe, F. 1998. The first simulation of an ozone QBO in a general circulation model. *Geophys. Res. Lett.* **25**, 3131–3134.

Niwano, M. and Shiotani, M. 2001. Quasi-biennial oscillation in vertical velocity inferred from trace gas data in the equatorial lower stratosphere. *J. Geophys. Res.* **106**, 7281–7290.

O'Sullivan, D. and Dunkerton, T. J. 1997. The influence of the quasi-biennial oscillation on global constituent distributions. *J. Geophys. Res.* **102**, 21,731–21,743.

Plumb, R. A. and Bell, R. C. 1982. A model of the quasi-biennial oscillation on an equatorial beta-plane. *Quart. J. R. Meteorol. Soc.* **108**, 335–352.

Politowicz, P. A. and Hitchman, M. H. 1997. Exploring the effects of forcing quasi-biennial oscillations in a two-dimensional model. *J. Geophys. Res.* **102**, 16,481–16,497.

Randel, W. J. and Wu, F. 1996. Isolation of the ozone QBO in SAGE II data by singular-value decomposition. *J. Atmos. Sci.* **53**, 2546–2559.

Randel, W. J., Wu, F., Russell, J. M., III, Roche, A. and Waters, J. W. 1998. Seasonal cycles and QBO variations in stratospheric CH_4 and H_2O observed in UARS HALOE data. *J. Atmos. Sci.* **55**, 163–185.

Randel, W. J., Wu, F., Swinbank, R., Nash, J. and O'Neill, A. 1999. Global QBO circulation derived from UKMO stratospheric analyses. *J. Atmos. Sci.* **56**, 457–474.

Reed, R. J. 1964. A tentative model of the 26-month oscillation in tropical latitudes. *Quart. J. R. Meteorol. Soc.* **90**, 441–466.

Rosenlof, K. H. 1995. The seasonal cycle of the residual mean meridional circulation in the stratosphere. *J. Geophys. Res.* **100**, 5173–5191.

Rosenlof, K. H. and Holton, J. R. 1993. Estimates of the stratospheric residual circulation using the downward control principle. *J. Geophys. Res.* **98**, 10,465–10,479.

Russell, J. M., III, Deaver, L. E., Luo, M., Cicerone, R. J., Park, J. H., Gordley, L. L., Toon, G. C., Gunson, M. R., Traub, W. A., Johnson, D. G., Jucks, K. W., Zander, R. and Nolt, I. G. 1996. Validation of hydrogen fluoride measurements made by the Halogen Occultation Experiment from the UARS platform. *J. Geophys. Res.* **101**, 10,163–10,174.

Ruth, S., Kennaugh, R., Gray, L. J. and Russell, J. M., III. 1997. Seasonal, semiannual, and interannual variability seen in measurements of methane made by the UARS Halogen Occultation Experiment. *J. Geophys. Res.* **102**, 16,189–16,199.

Takahashi, M. 1996. Simulation of the stratospheric quasi-biennial oscillation using a general circulation model. *Geophys. Res. Lett.* **23**, 661–664.

Takahashi, M. and Boville, B. A. 1992. A three-dimensional simulation of the equatorial quasi-biennial oscillation. *J. Atmos. Sci.* **49**, 1020–1035.

Trepte, C. R. and Hitchman, M. H. 1992. Tropical stratospheric circulation deduced from satellite aerosol data. *Nature* **355**, 626–628.

Wallace, J. M. 1973. General circulation of the tropical lower stratosphere. *Rev. Geophys. Space Phys.* **11**, 191–222.

Zawodny, J. M. and McCormick, M. P. 1991. Stratospheric aerosol and gas experiment II measurements of the quasi-biennial oscillations in ozone and nitrogen dioxide. *J. Geophys. Res.* **96**, 9371–9377.